Constrained PSK: Energy-Efficient Modulation for sub-THz Systems

Ismael Peruga Nasarre, Toni Levanen, and Mikko Valkama
Department of Electrical Engineering, Tampere University, Finland
Contact email: mikko.valkama@tuni.fi

***Abstract*—Deploying sub-THz frequencies for mobile communications is one timely research area, due to the availability of very wide and contiguous chunks of the radio spectrum. However, at such extremely high frequencies, there are large challenges related to, e.g., phase noise, propagation losses as well as to energy-efficiency, since generating and radiating power with reasonable efficiency is known to be far more difficult than at lower frequencies. To address the energy-efficiency and power amplifier (PA) nonlinear distortion related challenges, modulation methods and waveforms with low peak-to-average-power ratio (PAPR) are needed. To this end, a new modulation approach is formulated and proposed in this paper, referred to as constrained phase-shift keying (CPSK). The CPSK concept builds on the traditional PSK constellations, while additional constraints are applied to the time domain symbol transitions in order to control and reduce the PAPR of the resulting waveform. This new modulation is then compared with pulse-shaped $\pi/2$-BPSK and ordinary QPSK, in the discrete Fourier transform (DFT) spread orthogonal frequency division multiplexing (DFT-s-OFDM) context, in terms of the resulting PAPR distributions and the achievable maximum PA output power, subject to constraints in the passband waveform quality and out-of-band emissions. The obtained results show that the proposed CPSK approach allows for reducing the PAPR and thereon for achieving higher PA output powers, compared to QPSK, while still offering the same spectral efficiency. Overall, the CPSK concept offers a flexible modulation solution with controlled PAPR for the future sub-THz networks.**

***Index Terms*—5G New Radio (NR) evolution, sub-THz communications, energy-efficiency, modulation, DFT-s-OFDM, PAPR, power amplifiers.**

I. Introduction

Exploiting the sub-THz frequency bands in mobile radio networks has the potential to facilitate large amounts of new spectrum, and very wide contiguous channels, and thus substantial improvements in the radio access latency and data rates [1]–[3]. Thus, the third generation partnership project (3GPP) has recently started studies and work items for 5G New Radio (NR) evolution at beyond 52.6 GHz bands [3], [4], where one research and development target is to find a common waveform for the sub-THz communications. However, at such sub-THz frequencies, substantial implementation challenges appear, that include e.g. high levels of phase noise (PN) in oscillators as well as the limited ability to provide and radiate energy with reasonable power-efficiency and signal quality [5], [6]. Additionally, the path losses at sub-THz frequencies are severe [7], entailing the need for very large antenna gains and good power-amplifier (PA) efficiency such that feasible cell ranges and coverage could be supported.

In order to facilitate feasible power-efficiency through pushing the PA units towards deep saturation, waveforms with low peak-to-average power ratio (PAPR) are required, such that also sufficient signal quality in terms of error vector magnitude (EVM) can be achieved. PN mitigation is also an important research topic at sub-THz frequencies, however, in this paper the focus is on the development of energy-efficient low-PAPR modulations and waveforms. To this end, the currently supported waveforms in 5G NR are cyclic prefix orthogonal frequency division multiplexing (CP-OFDM) in downlink (DL) and uplink (UL), and discrete Fourier transform (DFT) spread OFDM (DFT-s-OFDM), also known as single-carrier frequency division multiple access (SC-FDMA), in the UL [8]. The current approach in 3GPP is to pursue the minimum possible changes to the current specifications when working for the 5G NR evolution towards the sub-THz regime. It is generally well known that DFT-s-OFDM has smaller PAPR than CP-OFDM [9], making it thus a more favorable candidate for both UL and DL at the sub-THz bands. For that reason, the modulation concepts and developments reported in this paper are carried out in the context of DFT-s-OFDM.

In this paper, we focus on the low-PAPR modulation advancements in the low spectral efficiency (SE) regime in the order of 1 to 2 bits/s/Hz. The reference modulations are pulse shaped $\pi/2$-BPSK [10] and QPSK, with 1 bit per sub-symbol and 2 bits per sub-symbol, respectively, already supported by the Third Generation Partnership Project (3GPP) Release- 15 (Rel-15) NR [11], while no solutions are currently available in 5G NR with SE between 1 and 2 bits/s/Hz and PAPR lower than QPSK. Motivated by this, a new constrained PSK (CPSK) modulation concept is proposed in this paper, which can facilitate SE of 1.5 or 2 bits/s/Hz, while having lower PAPR than QPSK. Technically, the main idea is to apply selected constraints in the waveform behavior between the consecutive symbol transitions, essentially limiting the set of available constellation points of the underlying PSK constellation per symbol instant. By using this approach, the PAPR of the signal can be efficiently controlled and significantly reduced, while also allowing to flexibly tailor the SE through the particular set of constraints and the underlying PSK constellation size.

This work was financially supported by Nokia Bell Labs and by the Finnish Funding Agency for Innovation under the project 5G FORCE. The work was also supported by the Academy of Finland under the grant #319994.

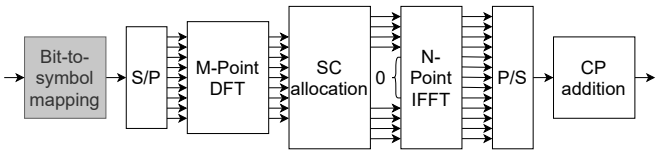

Fig. 1. DFT-s-OFDM processing framework. In this work, the emphasis is on the bit-to-symbol mapping, a.k.a., data modulation, illustrated in grey.

Extensive numerical results are also provided in the paper where the proposed CPSK concept is compared against the $\pi/2$-BPSK and QPSK based reference modulations, in terms of the PAPR distributions and the achievable PA output powers for given EVM and out-of-band emission requirements. The obtained results show that the proposed CPSK approach allows for efficiently reducing the PAPR and thereon for achieving higher PA output powers, compared to the reference methods.

It is noted that different recent works have considered new modulations or related techniques to control PAPR, see, e.g., [12]–[15]. However, to decrease the PAPR, these methods impose inherent SE penalty which makes them less appealing.

The rest of the paper is organized as follows: Section II shortly reviews the DFT-s-OFDM principle as well as the $\pi/2$-BPSK and QPSK based reference modulations. Additionally, the proposed CPSK modulation concept is described. In Section III, the performance evaluations methods, assumptions and the utilized models are described. Then, in Section IV, the obtained numerical results are presented and analyzed in order to evaluate the performance of the proposed CPSK approach and to compare it against the $\pi/2$-BPSK and QPSK reference solutions. Finally, Section V draws the conclusions.

II. Low-PAPR Waveforms: Reference Methods and Proposed CPSK Approach

A. DFT-s-OFDM Principle and Reference Modulations

The basic DFT-s-OFDM based processing block-diagram is shown in Fig. 1, performing a DFT of size M over the complex input symbols, assigning them to M of the N available subcarriers and performing an inverse fast-Fourier-transform (IFFT) of size N. After the IFFT, a cyclic prefix (CP) is added to each DFT-s-OFDM symbol. As earlier noted, the reference modulations available in 5G NR are pulse shaped $\pi/2$-BPSK, referred to in this work as [1+D]$\pi/2$-BPSK, and QPSK. Even though these are well-known and widely used, we shortly express them for completeness of presentation, together with well-known $\pi/4$-QPSK, while the proposed CPSK principle is then described in subsection II-B.

In general, the bit-to-symbol mapper takes a block of input bits and produces a block of complex-valued modulated data symbols. To obtain the symbols for the [1+D]$\pi/2$-BPSK, first a $\pi/2$ rotation is applied to every other symbol over a block of basic BPSK symbols, expressed as

$$s_i^{\pi/2-\text{BPSK}} = e^{j\frac{\pi}{2}\text{mod}(i,2)}[1-2b(i)], \quad (1)$$

where $b(i) \in \{0,1\}$ is the ith bit, and $\text{mod}(i,2)$ is the modulo two operation over the integer symbol index $i \in \{0,1,...,M-1\}$. It is noted that for every even symbol index, the symbols are on the real axis, while for odd symbol indices, the symbols are on the imaginary axis. Finally, to obtain the [1+D]$\pi/2$-BPSK symbols, a combination of two consecutive symbols over the same DFT-s-OFDM symbol is performed, expressed as

$$s_i^{[1+D]\pi/2-\text{BPSK}} = \frac{s_i^{\pi/2-\text{BPSK}} + s_{\text{mod}(i-1,M)}^{\pi/2-\text{BPSK}}}{\sqrt{2}}. \quad (2)$$

The $1+D$ shaping filter essentially acts as a root raised cosine (RRC) filter in frequency domain, shaping the spectrum of the signal [16]. The output constellation resembles now the familiar QPSK modulation since a real symbol is combined with an imaginary symbol. However, the information bearing signal is still only in one domain, and the signal component in the other domain can be considered as inter-symbol-interference (ISI) that is deliberately introduced to mitigate PAPR. Because the information bearing signal and ISI are in different domains, their separation is straightforward in the receiver. In general, the inclusion of the $\pi/2$ rotation and the spectral shaping filter helps to reduce the PAPR of the signal [16].

QPSK is another common digital modulation with a constellation size of 4 symbols, each carrying 2 bits. The mapping from bits to symbol is here defined as

$$s_i^{\text{QPSK}} = \frac{1}{\sqrt{2}}[(2b(2i)-1)+j(2b(2i+1)-1)]. \quad (3)$$

Additionally, a well-known variant of QPSK is the so-called $\pi/4$-QPSK approach, which basically follows a similar idea as the $\pi/2$-BPSK modulation, where every other symbol is rotated by $\pi/4$ radians in order to avoid 180º phase changes between two consecutive symbols. The generation of $\pi/4$-QPSK modulated symbols is straightforward once the basic QPSK symbols are obtained, expressed here as

$$s_i^{\pi/4-\text{QPSK}} = e^{j\frac{\pi}{4}\text{mod}(i,2)} s_i^{\text{QPSK}}. \quad (4)$$

B. Proposed Constrained PSK (CPSK) Principle

The constrained PSK (CPSK) modulation is a new approach proposed in this paper, with the main goal of allowing for flexible PAPR and spectral efficiency control. This concept builds on traditional PSK constellations of different sizes, where the baseline symbols are placed at the unit circle and with a phase of $\frac{2\pi k}{K}$ radians for the symbol index $k \in \{0,1,...,K-1\}$ with K denoting the constellation size. Then, additional constraints are applied in time domain to the assigned symbols depending on the target spectral efficiency and the selected optimization target. As the optimization target in this paper is to control the PAPR of the transmitted signal, the constraints are designed to restrict the possible symbol transitions between two different symbol instants. More specifically, the symbol transitions are constrained to one or more of the closest neighbors of the currently prevailing symbol. This basic concept is illustrated in Fig. 2, for cases where the underlying basic constellation size is $K = 6$.

Specifically, in this work, two constraints with different spectral efficiencies are studied in further details – one which

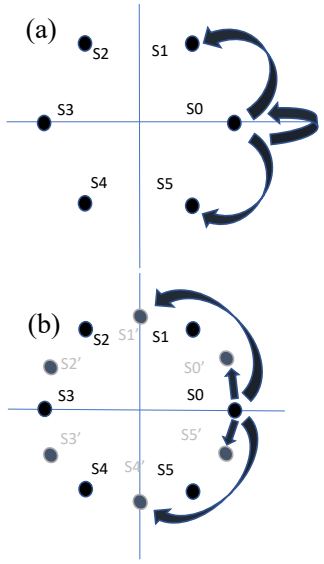

Fig. 2. Illustration of allowed symbol transitions for (a) C6PSK/3 and (b) C6PSK/4, including a rotation of $\pi/6$ for every other symbol.

TABLE I
EXAMPLE MAPPING TABLE FOR C6PSK/3. FOR EACH SEQUENCE OF INPUT BITS, THE MAPPING TABLE DEFINES THE TWO FOLLOWING TRANSMITTED SYMBOLS, BASED ON THE PREVIOUS SYMBOL.

	Previous symbol											
Input bits	$\mathbf{s_0}$		$\mathbf{s_1}$		$\mathbf{s_2}$		$\mathbf{s_3}$		$\mathbf{s_4}$		$\mathbf{s_5}$	
000	s_0	s_1	s_1	s_2	s_2	s_3	s_3	s_4	s_4	s_5	s_5	s_0
001	s_0	s_5	s_1	s_0	s_2	s_1	s_3	s_2	s_4	s_3	s_5	s_4
010	s_1	s_2	s_2	s_3	s_3	s_4	s_4	s_5	s_5	s_0	s_0	s_1
011	s_5	s_4	s_0	s_5	s_1	s_0	s_2	s_1	s_3	s_2	s_4	s_3
100	s_1	s_0	s_2	s_1	s_3	s_2	s_4	s_3	s_5	s_4	s_0	s_5
101	s_5	s_0	s_0	s_1	s_1	s_2	s_2	s_3	s_3	s_4	s_4	s_5
110	s_1	s_1	s_2	s_2	s_3	s_3	s_4	s_4	s_5	s_5	s_0	s_0
111	s_5	s_5	s_0	s_0	s_1	s_1	s_2	s_2	s_3	s_3	s_4	s_4

TABLE II
EXAMPLE MAPPING TABLE FOR C6PSK/4. FOR INPUT BITS "11", THE GIVEN CONSTELLATION POINTS CORRESPOND TO EVEN/ODD SYMBOL INDEX.

	Previous symbol					
Input bits	$\mathbf{s_0}$	$\mathbf{s_1}$	$\mathbf{s_2}$	$\mathbf{s_3}$	$\mathbf{s_4}$	$\mathbf{s_5}$
00	s_0	s_1	s_2	s_3	s_4	s_5
01	s_1	s_2	s_3	s_4	s_5	s_0
10	s_5	s_0	s_1	s_2	s_3	s_4
11	s_2/s_4	s_3/s_5	s_4/s_0	s_5/s_1	s_0/s_2	s_1/s_3

allows for 3 possible symbol transitions (noted as CKPSK/3), and another which allows for 4 possible transitions (noted as CKPSK/4). To this end, CKPSK/3 modulations can carry $\log_2(3) \approx$1.5 bits per symbol, whereas CKPSK/4 modulations allow for 2 bits per symbol, while the baseline constellation size K is another design parameter that has an impact on PAPR. In general, by increasing the value of K, under the given constraints, the instantaneous envelope of the CPSK modulated signals can be forced to be closer and closer to the unit circle, reflecting smaller and smaller PAPR.

In general, to generate the CPSK symbols, the input bits can be divided into groups to form one or multiple CPSK blocks, where the first symbol of the block can be, e.g., freely chosen without following the given constraint between CPSK blocks. For example, if CPSK is used with DFT-s-OFDM, one CPSK block may correspond to all of the allocated sub-symbols inside a DFT-s-OFDM symbol. It is noted that the inclusion of CPSK modulation in the context of DFT-s-OFDM does not imply any additional processing blocks or essentially increase the complexity of the modulator, since the only difference with respect to traditional modulations is on the bit-to-symbol mapping. These mappings are explicitly addressed next.

1) Bit-to-symbol mapping for CKPSK/3: The CPSK modulations with 3 options carry 1.5 bits per symbol, which in practice is translated into 3 bits being mapped into 2 symbols. Fig. 2(a) shows an example of possible transitions for a constraint allowing 3 possible symbols at every time instant when the base constellation is 6PSK. As can be noted, if the previous symbol was s_0, then the next possible symbol can be either s_0, s_1 or s_5. In other words, with the given 3 option constraint, the allowed transitions are: staying in the same symbol (s_0, s_0), or move to one of the closest neighbors, corresponding to transitions (s_0, s_1) or (s_0, s_5). The determination of closest neighbor can be based on, e.g., Euclidean distance or angular distance between constellation points.

In order to perform the bit-to-symbol mapping, one practical approach is the use of mapping tables. An example of a mapping table is shown in Table I for C6PSK/3. We note that this mapping is just one example, and that the exact bit-to-symbol mapping can be defined independently for each base constellation size, or based on the applied constraints. Assuming M symbols per CPSK block, corresponding to $B = \frac{3}{2}M$ bits per CPSK block, the mapping for 3 options case can be described as follows:

1) The B bits are divided into groups of 3 bits.
2) Based on the CPSK block index (b_{CPSK}), the column $s_{\text{mod}(b_{\text{CPSK}},K)}$ is used. This is in order to have different starting symbol for each CPSK block.
3) The 3 input bits give the row in the Table I that contains the pair of symbol to be sent.
4) The second symbol selected from the Table I at step 3 defines the next column used for mapping the next 3 input bits.
5) Steps 3 and 4 are repeated until all the bits of the b_{CPSK}th block are mapped to CPSK symbols.

2) Bit-to-symbol mapping for CKPSK/4: The CPSK modulations with 4 options carry 2 bits per symbols. Fig. 2(b) shows an example of possible transitions for 6PSK/4, with a constraint allowing 4 possible symbols per time instant. To further reduce the PAPR in the 4 options case, a base constellation rotation of π/K radians is applied to every other symbol. Similar to any rotated modulation, constellation rotation can be applied without affecting the detection performance, but has a positive impact on the PAPR distribution. Therefore, black and gray symbols in Fig. 2(b) are used for even and odd time

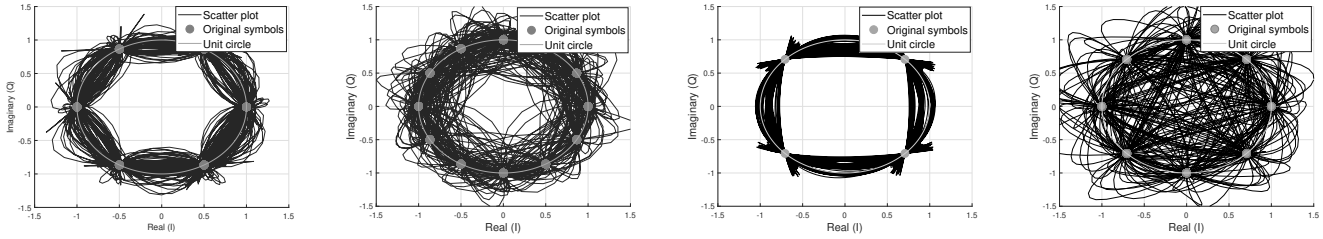

(a) (b) (c) (d)

Fig. 3. I/Q scatter diagram examples for (a) C6PSK/3, (b) C6PSK/4, (c) [1+D]$\pi/2$-BPSK, and (d) $\pi/4$-QPSK modulations.

instants, respectively.

Similar to the 3 options case, the bit-to-symbol mapping can be defined through the mapping tables. An example of a mapping table for 4 options case is shown in Table II. Noting the last row in Table II, the allowed symbol transition varies for even and odd symbol indices in order to avoid constant rotation into a specific direction over a block of CPSK symbols, that would basically be observed as a frequency shift in the output spectrum. In general, with the 4 options constraints, the possible transitions are: staying in the same symbol, (s_0, s'_0), move to one of the closest neighbors, (s_0, s'_1) or (s_0, s'_5), or to one of the second-closest neighbor from one side, (s_0, s'_4).

In general, assuming M symbols per CPSK block, with $B = 2M$ bits per CPSK block, the mapping for 4 options case can be described as follows:

1) The B bits are divided in groups of 2 bits.
2) Based on the CPSK block index (b_{CPSK}), the column $s_{\text{mod}(b_{\text{CPSK}},K)}$ is used.
3) The 2 input bits give the row in the Table II that contains the symbol to be sent (for even/odd symbol index).
4) The previous symbol selected from the Table II at step 3 defines the next column used for mapping the next 2 input bits.
5) Steps 3 and 4 are repeated until all the bits of the b_{CPSK}th block are mapped.

To further illustrate the effects of the constraints on the signal, and to compare the CPSK principle with the reference modulations, Fig. 3 shows the I/Q scatter diagrams of the C6PSK with 3 and 4 options, pulse shaped $\pi/2$-BPSK, and $\pi/4$-QPSK modulations. It can be observed that the applied constraints result to avoiding the zero-crossings, and that the signal stays close to the unit circle. The I/Q scatter diagram of the pulse-shaped $\pi/2$-BPSK, in Fig. 3(c), shows even further reduced variations in the signal envelope. It can also be observed that even though the $\pi/4$-QPSK avoids 180 degree phase jumps between consecutive symbols, there is no clear opening in the middle of the scatter diagram and also that clearly higher peaks are present in the signal compared to the other modulations. We note that for C6PSK/4, pulse shaped $\pi/2$-BPSK, and $\pi/4$-QPSK modulations, the number of original symbol constellation points is doubled due to the base constellation rotation every other time instant.

III. Performance Evaluation Scenarios and Assumptions

We next shortly describe the main performance evaluation scenarios and related assumption. The main metric used to evaluate the transmitter-side energy-efficiency of the waveforms is the sample-wise PAPR distribution. This sample-wise PAPR is defined as the ratio between the instantaneous squared envelope and the corresponding average power of the signal, as

$$PAPR(n) = \frac{|x(n)|^2}{\frac{1}{N}\sum_{l=0}^{N-1}|x(l)|^2}. \quad (5)$$

where $x(n)$ denotes the complex sample at time-instant n, while the overall signal length in samples is denoted by N. Once the sample-wise PAPR values are obtained for the different considered waveforms, their complementary cumulative distribution functions (CCDFs) are calculated and utilized for modulation comparison. Specifically, the PAPR values at 1% point are used for explicit quantitative comparisons.

To further quantify and account for the practical benefits of CPSK, the maximum PA output powers of the different waveforms are also evaluated. The PA model used in this work is the modified Rapp model defined in [17] for IEEE 802.11ad operating at 60 GHz ISM band, since it is the only commonly available PA model for evaluations with a frequency of operation close to sub-THz range. After applying the PA model, the power spectral density (PSD) of the output signal, with a resolution bandwidth of 1 MHz, is compared to a modified IEEE 802.11ad spectrum mask [18]. For evaluations, 180 physical resource blocks (PRB) are allocated, where each PRB corresponds to 12 subcarriers. The used subcarrier spacing (SCS) is 960 kHz, four times larger than currently supported by the 5G New Radio in frequency range 2 (FR2) [19]. We have chosen this value since it is expected that the supported SCSs have to be larger for sub-THz frequencies in order to combat the effects of PN and to support wider channel bandwidths [20]. Therefore, the allocated bandwidth corresponds to 2.0736 GHz, designed to fit into the 2.16 GHz channel bandwidth currently used by IEEE 802.11ad. Because the assumed bandwidth utilization, corresponding to 96%, is higher in our model than in IEEE 802.11ad, we have modified the mask in such a manner that passband is extended to fit the transmitted signal and the -17 dBr point aligns with the first

active subcarrier of the neighboring channel, corresponding to 1.1232 GHz distance from the carrier frequency.

In addition to the emission mask, adjacent channel leakage ratio (ACLR), as defined in [21], is also evaluated. Considering the UL direction in the evaluations, the used ACLR limit is 17 dB, corresponding to the most restrictive case for the UE in FR2 [21]. However, seeing the evolution of the ACLR limits from FR1 [22] to FR2 [21], it is expected that the ACLR limits become even more relaxed in sub-THz communications. Also, the EVM is evaluated by using a test receiver, and compared to the limits defined in [21], which correspond to 30% for $\pi/2$-BPSK and 17.5% for QPSK. For reference, the EVM limit used for CPSK modulations was 17.5%. However, it could be expected that the CPSK modulations with base constellation sizes greater than 4 may have more restrictive EVM limits. Nevertheless, in all the performed evaluations, their EVM values are far below such limit. Furthermore, following the occupied bandwidth requirement from [21], we have ensured that 99% of the signal power is within the channel bandwidth.

To summarize, the maximum achievable PA output power is obtained after the signal passes through the PA model with maximum gain, while still fulfilling all the following requirements:

1) The filtered PSD is below the emission mask.
2) 99 % of the signal power is inside the channel bandwidth (occupied bandwidth, OBW).
3) ACLR is greater than 17 dB.
4) EVM is below the specified limit.

IV. Obtained Performance Results and Analysis

A. Sample-wise PAPR Distributions

The PAPR distributions for the different considered modulations are shown in Fig. 4. The plotted PAPR CCDFs are obtained by analyzing 10000 DFT-s-OFDM symbols with four times oversampling in order to obtain reliable information about the signal peaks [23]. As can be observed, CPSK modulations provide a range of PAPR that lies between the PAPR of [1+D]$\pi/2$-BPSK and that of QPSK, depending on the modulation order or the number of options. We can also observe that in the evaluation point of a 1% probability, the [1+D]$\pi/2$-BPSK has a PAPR of 1.55 dB while $\pi/4$-QPSK presents a PAPR of 4.5 dB, which is essentially the same as that of plain QPSK. Therefore, as an additional observation, we can conclude that the $\pi/4$ rotation over QPSK does not help to reduce the PAPR of the signal. Increasing the base constellation size for CPSK/3 allows to decrease the PAPR at 1% probability from 3.55 dB with C4PSK/3 down to 1.55 dB with C8PSK/3. Importantly, this means that with C8PSK/3, we are able to reach the [1+D]$\pi/2$-BPSK PAPR performance but with higher SE. On the other hand, it is also observed that CPSK/4 modulations have smaller PAPR than QPSK while still providing the same SE. For example, C5PSK/4 PAPR at 1% probability level is 3.7 dB, which is already 0.8 dB smaller than that of QPSK.

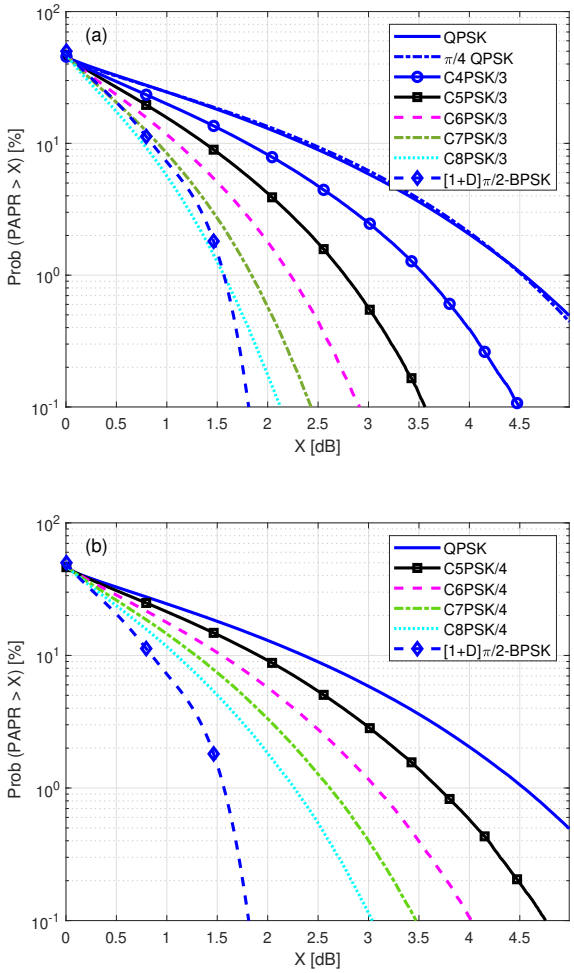

Fig. 4. CCDFs of sample-wise PAPR, comparing pulse shaped $\pi/2$-BPSK, QPSK and $\pi/4$-QPSK with (a) CPSK/3 modulations (with different baseline constellation orders) and (b) CPSK/4 modulations (with different baseline constellation orders).

B. Achievable Maximum PA Output Power

Using the evaluation assumptions and the PA model described in Section III, the maximum PA output powers, per modulation, are next obtained. These evaluations are made to explicitly demonstrate the effect of the PA input signal PAPR on the maximum achievable PA output power, while still respecting the spectrum emission mask, having 99% of the power residing inside the channel bandwidth as well as fulfilling both the ACLR and EVM limits. Maximizing the PA output power is important to maximize the power efficiency of the transmitter and the cell coverage, which is directly dependent on the obtained PA output power.

First, to illustrate and visualize the effects of the PA on the signals, Fig. 5 shows the filtered PSD of the C6PSK/4 before and after passing through the PA, while the modified spectrum mask is also depicted for reference. One interesting feature of the CPSK signals is that the majority of the signal power is located at the center of the channel, giving the PSD a tilted or filtered low-pass spectral shape. It can be observed

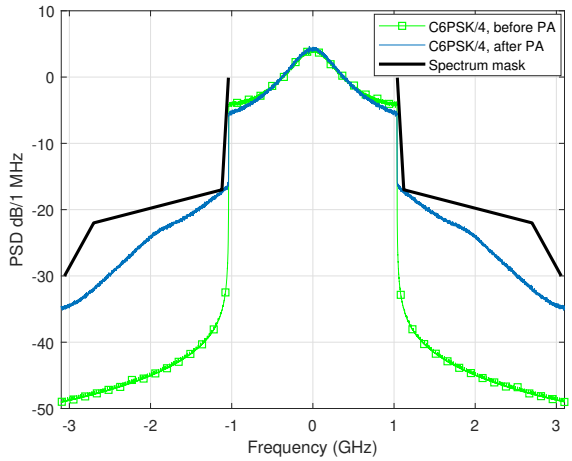

Fig. 5. Filtered PSD of C6PSK/4 before and after passing through the PA. Also the modified IEEE 802.11ad emission mask is shown for reference.

TABLE III
OBTAINED MAXIMUM PA OUTPUT POWERS AND OTHER SIGNAL METRICS

Modulation	SE [bps/Hz]	PAPR @1% [dB]	EVM [%]	Max. PA output power [dBm]	Limiting factor
[1-D]π/2-BPSK	1	1.55	14.4	**+25.26**	Sat. level
QPSK	2	4.50	8.9	+21.09	Mask
$\pi/4$-QPSK	2	4.50	8.9	+21.10	Mask
C4PSK/3	1.5	3.56	9.2	+23.28	OBW
C5PSK/3	1.5	2.77	8.9	+24.73	Mask
C6PSK/3	1.5	2.21	7.9	**+25.26**	Sat. level
C7PSK/3	1.5	1.83	6.6	**+25.26**	Sat. level
C8PSK/3	1.5	1.55	6.1	**+25.26**	Sat. level
C5PSK/4	2	3.67	9.6	+22.79	OBW
C6PSK/4	2	3.06	9.6	+24.17	Mask
C7PSK/4	2	2.62	10.2	+25.00	Mask
C8PSK/4	2	2.26	8.8	**+25.26**	Sat. level

from the figure that after the PA, the out-of-band emissions increase significantly and the PSD is mainly limited by the nearest corner points of the mask, corresponding to the -17 dBr requirements.

Table III shows the maximum PA output powers obtained for all the studied modulations, while also collects the corresponding SE values, PAPR values at 1% probability point and the EVM values. We can clearly observe the benefits that the reduction of PAPR brings in terms of the maximum achievable PA output power. As an example, QPSK with 4.50 dB of PAPR at 1% probability level achieves +21.09 dBm of output power, while C5PSK/4 achieves +22.79 dBm output power. This reflects 1.7 dB higher output power with 0.83 dB smaller PAPR at 1% probability level. As pointed out before, the $\pi/4$ rotation over QPSK does not bring any essential benefits, something that can also be observed from the table. It is also noted that pulse shaped $\pi/2$-BPSK reaches the saturation power of the PA, corresponding to +25.26 dBm. The reason for higher EVM with pulse shaped $\pi/2$-BPSK is due to the assumption of transparent transmitter processing, in which case the receiver is unaware of the used pulse shaping function and this leads into considerable noise enhancement in the receiver equalization process before EVM evaluation.

It can also be observed that under the current evaluation scenario, the PA output power of all the CPSK modulations is higher than the QPSK reference, and several of them are reaching the saturation power of the PA while having higher SE than pulse shaped $\pi/2$-BPSK. This implies that it is indeed technically feasible to adopt the proposed CPSK modulation principle, and thus to extend the current set of supported 5G NR modulations, in order to achieve improved transmission powers when compared to QPSK, while operating with SE of 1.5 bits or 2 bits. These are findings of substantial importance, when the 5G NR technology evolution progresses towards the sub-THz frequencies.

C. Excursion: CPSK as Analysis Waveform Engine

We next shortly discuss the additional flavor of the CPSK waveform family, as an analysis tool in PA measurements and modeling. To this end, it was shown in Section IV-A that the PAPR of the CPSK signals can be decreased by increasing the base constellation size. We next study and pursue the behavior of the PAPR values at 1% probability point with respect to the base constellation size K, or correspondingly the maximum phase difference between two constellation points, or two consecutive symbols for CPSK/3 modulations, corresponding to $2\pi/K$ radians.

Evaluating the PAPR at 1% probability level, Fig. 6(a) shows the evolution of the PAPR as a function of the constellation size, while Fig. 6(b) illustrates the PAPR with respect to the maximum phase difference between the two consecutive symbols. It can be observed that when the constellation size increases, the envelope becomes more and more constant, and therefore, the PAPR decreases. Interestingly, these results also show that the PAPR values at 1% point is a linear function of the phase difference between 2 consecutive CPSK symbols.

Obviously, increasing the constellation size to higher values is not suitable for communications due to the fact that neighbor symbols become closer and closer, and thus the detection performance would be degraded or the corresponding SNR requirements for reliable detection would increase. However, it is clear from the results that it is possible to have very accurate control of the PAPR that the CPSK waveform presents. Such accurate PAPR control can facilitate flexible analysis of different PA models, or corresponding actual PA hardware samples, by adjust the CPSK modulation to match the desired PAPR. This opens new possibilities to improve our understanding on what is sufficiently low PAPR for a specific PA technology or PA model.

V. CONCLUSION

In this paper, a new energy-efficient modulation concept, referred to as CPSK, was proposed and described. The CPSK approach builds on the idea of constrained or coded modulation where properly tailored constraints are applied between two consecutive symbol instants such that the PAPR can be controlled and reduced. The proposed method was compared with pulse shaped $\pi/2$-BPSK and QPSK reference

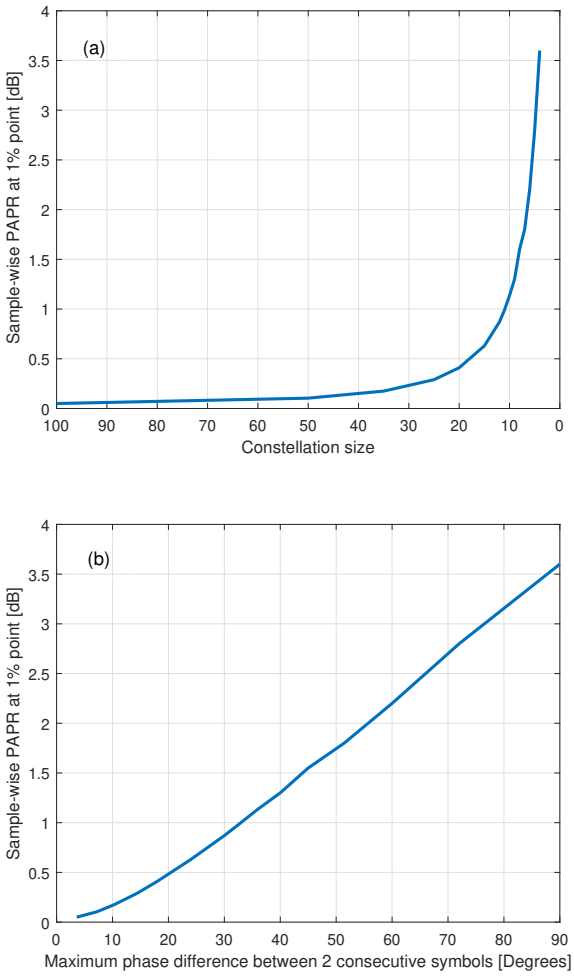

Fig. 6. Effect of the base constellation size on the sample-wise PAPR at 1% probability level for CPSK/3 modulation with respect to the (a) constellation size or (b) maximum phase difference between 2 consecutive symbols.

modulations, in the context of DFT-s-OFDM based radio access, in terms of the achievable PAPR and maximum PA output power, such that the selected EVM and out-of-band emission limits are fulfilled. The obtained results show that the CPSK principle allows to efficiently reduce the PAPR of the waveform, and therefore, to increase the maximum PA output power under the given passband quality and emission requirements. Specifically, CPSK modulations carrying 2 bits per symbol were shown to achieve higher maximum output power than QPSK, potentially even reaching the full saturation level of the PA – similar to the pulse shaped $\pi/2$-BPSK – but with higher spectral efficiency. Finally, an additional potential use of the CPSK waveforms was shortly discussed, capitalizing the flexibly tunable PAPR of the proposed waveform family through the size of the underlying baseline PSK constellation and the applied constraints. This can, e.g., allow flexible testing of different PA samples and extracting the corresponding PA models, under different input PAPRs, which are needed to test different candidate waveforms for sub-THz communications within a common evaluation frame.

REFERENCES

[1] S. Rangan, T. S. Rappaport, and E. Erkip, "Millimeter-wave cellular wireless networks: Potentials and challenges," *Proceedings of the IEEE*, vol. 102, no. 3, pp. 366–385, March 2014.

[2] Ian F. Akyildiz, Josep Miquel Jornet, and Chong Han, "Terahertz band: Next frontier for wireless communications," *Physical communication*, vol. 12, no. 1, pp. 16–32, Sept. 2014.

[3] "3GPP TR 38.807 V16.0.0, "Study on requirements for NR beyond 52.6 GHz", Tech. Spec. Group Radio Access Network. Rel-16."

[4] "3GPP TR 38.805 V14.0.0, "Study on New Radio access technology; 60 GHz unlicensed spectrum", Tech. Spec. Group Radio Access Network. Rel-14," Mar. 2017.

[5] "3GPP TR 38.803 V14.2.0, "Study on new access technology: Radio Frequency (RF) and co-existence aspects", Tech. Spec. Group Radio Access Network. Rel-14," Sept. 2017.

[6] P. M. Asbeck, N. Rostomyan, M. Özen, B. Rabet, and J. A. Jayamon, "Power Amplifiers for mm-Wave 5G Applications: Technology Comparisons and CMOS-SOI Demonstration Circuits," *IEEE Transactions on Microwave Theory and Techniques*, vol. 67, no. 7, pp. 3099–3109, Jul. 2019.

[7] J. M. Jornet and I. F. Akyildiz, "Channel Modeling and Capacity Analysis for Electromagnetic Wireless Nanonetworks in the Terahertz Band," *IEEE Transactions on Wireless Communications*, vol. 10, no. 10, pp. 3211–3221, Oct. 2011.

[8] E. Dahlman, S. Parkvall, and J. Sköld, *5G NR: The Next Generation Wireless Access Technology*, 1st ed. Academic Press, 2013.

[9] ——, *4G: LTE/LTE-Advanced for Mobile Broadband*, 1st ed. Academic Press, 2013.

[10] "3GPP TSG RAN WG1, "R1-1701180 Comparison of pi/2 BPSK with and without frequency domain pulse shaping: Results with PA model", IITH, CEWiT, IITM, Tejas Networks," Jan. 2017.

[11] "3GPP TS 38.211 V16.0.0, "Physical channels and modulation", Tech. Spec. Group Radio Access Network. Rel-16," Dec. 2019.

[12] Y. Levinbook, D. Ezri, and E. Melzer, "Low-PAPR OFDM-based waveform for fifth-generation cellular communications," in *2017 IEEE International Conference on Microwaves, Antennas, Communications and Electronic Systems (COMCAS)*, Nov. 2017, pp. 1–6.

[13] S. C. Thompson, A. U. Ahmed, J. G. Proakis, J. R. Zeidler, and M. J. Geile, "Constant Envelope OFDM," *IEEE Transactions on Communications*, vol. 56, no. 8, pp. 1300–1312, August 2008.

[14] T. F. Rahman, C. Sacchi, S. Morosi, A. Mazzinghi, and N. Bartolomei, "Constant-Envelope Multicarrier Waveforms for Millimeter Wave 5G Applications," *IEEE Transactions on Vehicular Technology*, vol. 67, no. 10, pp. 9406–9420, Oct 2018.

[15] R. Mulinde, T. F. Rahman, and C. Sacchi, "Constant-envelope SC-FDMA for nonlinear satellite channels," in *2013 IEEE Global Communications Conference (GLOBECOM)*, Dec 2013, pp. 2939–2944.

[16] "3GPP TSG RAN WG4 Meeting #82, "Potential Response to LS on pi/2 BPSK with frequency domain pulse shaping", IITH, CEWiT, IITM, Tejas Networks," Feb. 2017.

[17] "IEEE P802.11 Wireless LANs, "TGad Evaluation Methodology", doc.: IEEE 802.11-09/0296r16," Jan. 2009.

[18] IEEE, "IEEE Standard for Information technology–Telecommunications and information exchange between systems–Local and metropolitan area networks–Specific requirements-Part 11: Wireless LAN Medium Access Control (MAC) and Physical Layer (PHY) Specifications Amendment 3: Enhancements for Very High Throughput in the 60 GHz Band," *IEEE Std 802.11ad-2012*, pp. 1–628, Dec 2012.

[19] "3GPP TS 38.104 v15.4.0, "NR; Base Station (BS) radio transmission and reception", Tech. Spec. Group Radio Access Network, Rel. 15," Dec. 2018.

[20] T. Levanen, O. Tervo, K. Pajukoski, M. Renfors, and M. Valkama, "Mobile communications beyond 52.6 GHz: Waveforms, numerology, and phase noise challenge," *CoRR*, Dec. 2019. [Online]. Available: http://arxiv.org/abs/1912.09072

[21] "3GPP TS 38.101-2 V16.2.0, "User Equipment (UE) radio transmission and reception; Part 2: Range 2 Standalone", Tech. Spec. Group Radio Access Network. Rel-16," Dec. 2019.

[22] "3GPP TS 38.101-1 V16.2.0, "User Equipment (UE) radio transmission and reception; Part 1: Range 1 Standalone", Tech. Spec. Group Radio Access Network. Rel-16," Dec. 2019.

[23] H. Ochiai and H. Imai, "Performance analysis of deliberately clipped OFDM signals," *IEEE Trans. Commun.*, vol. 50, pp. 89–101, Jan 2002.